

Estimating the air shower X_max from radio measurements

Benoît Revenu, Richard Dallier, A. Escudie, D. García-Fernández, Lilian Martin

▶ **To cite this version:**

Benoît Revenu, Richard Dallier, A. Escudie, D. García-Fernández, Lilian Martin. Estimating the air shower X_max from radio measurements. 26th Extended European Cosmic Ray Symposium and 35th Russian Cosmic Ray Conference, Jul 2018, Barnaul, Russia. pp.012030, 10.1088/1742-6596/1181/1/012030 . hal-02088628

HAL Id: hal-02088628
https://hal.science/hal-02088628

Submitted on 5 Aug 2020

HAL is a multi-disciplinary open access archive for the deposit and dissemination of scientific research documents, whether they are published or not. The documents may come from teaching and research institutions in France or abroad, or from public or private research centers.

L'archive ouverte pluridisciplinaire **HAL**, est destinée au dépôt et à la diffusion de documents scientifiques de niveau recherche, publiés ou non, émanant des établissements d'enseignement et de recherche français ou étrangers, des laboratoires publics ou privés.

Journal of Physics: Conference Series

PAPER • **OPEN ACCESS**

Estimating the air shower X_{max} from radio measurements

To cite this article: B. Revenu *et al* 2019 *J. Phys.: Conf. Ser.* **1181** 012030

View the article online for updates and enhancements.



IOP ebooks™

Bringing together innovative digital publishing with leading authors from the global scientific community.

Start exploring the collection–download the first chapter of every title for free.

This content was downloaded from IP address 163.9.11.179 on 05/08/2020 at 13:06

IOP Conf. Series: Journal of Physics: Conf. Series 1181 (2019) 012030 doi:10.1088/1742-6596/1181/1/012030

Estimating the air shower $X_{\mathbf{max}}$ from radio measurements

B. Revenu[1,3], R. Dallier[1,3], A. Escudie[1], D.García-Fernández[1], L. Martin[1,3]

[1] Subatech, Institut Mines-Telecom Atlantique, CNRS, Université de Nantes, Nantes, France
[2] Nantes, France
[3] Unité Scientifique de Nançay, Observatoire de Paris, CNRS, PSL, UO/OSUC, Nançay, France

E-mail: revenu@in2p3.fr

Abstract. It is possible to use the radio signal emitted by air showers to estimate the primary cosmic ray characteristics, in particular its nature through the shower $X_{\max}$. The electric field emitted by air showers is computed assuming an atmospheric model; we need to know the air density and refractive index since these parameters have and influence on the development of the shower and the emitted electric field. We can get an unbiased estimation using the Global Data Assimilation System (GDAS) to compute the precise atmospheric conditions at the time and location an event is detected. We show how to use these data.

1. Introduction

Many experiments are using the radio technique in addition to older technologies like a fluorescence telescope or a surface detector [1, 2, 3]. The radio signal has a duty cycle close to 100% and it permits to estimate directly the shower $X_{\max}$ with an uncertainty similar to what is obtained with a fluorescence telescope. We use the signal in the band 20-80 MHz where the electric field is coherent (the exact coherence band depends on the shower geometry). The estimation of the primary cosmic ray characteristics is performed by a comparison between the electric field measurements (amplitude, polarization, spectrum) with the theoretical expectation from simulation codes [4, 5, 6]. These codes are able to compute the electric field emitted by a shower as a function of time for any observer position. They all need as input the shower geometry (zenith θ, azimuth ϕ), the nature of the primary cosmic ray and its energy. After the first interaction at the atmospheric depth X_1, the secondary particles of the shower are created and tracked along their trajectory in the atmosphere. The electric field is computed for each of these particles and summed up to get the total electric field at the observer location. The propagation is driven by the medium and the first key ingredient is the air density $\rho_{\text{air}}(z)$ at every position of the secondary particles, i.e. for each altitude z, if we assume the atmosphere density only depends on z at fixed time. The second key ingredient is the air refractive index η


Content from this work may be used under the terms of the Creative Commons Attribution 3.0 licence. Any further distribution of this work must maintain attribution to the author(s) and the title of the work, journal citation and DOI.
Published under licence by IOP Publishing Ltd

which appears explicitely in the electric field formula (see [7] for the full derivation):

$$\mathbf{E}(\mathbf{x},t) = \frac{1}{4\pi\epsilon}\int \mathrm{d}^3x' \left\{ \left[\frac{\rho(\mathbf{x}',t')\mathbf{r}}{R^2(1-\eta\beta\cdot\mathbf{r})}\right]_{\mathrm{ret}} + \frac{\eta}{c}\frac{\partial}{\partial t}\left[\frac{\rho(\mathbf{x}',t')\mathbf{r}}{R(1-\eta\beta\cdot\mathbf{r})}\right]_{\mathrm{ret}} - \frac{\eta^2}{c^2}\frac{\partial}{\partial t}\left[\frac{\mathbf{J}(\mathbf{x}',t')}{R(1-\eta\beta\cdot\mathbf{r})}\right]_{\mathrm{ret}} \right\}. \quad (1)$$

This is the expected value at the observers coordinates $\mathbf{x}, t$ from the charge density ρ, current $\mathbf{J}$, $\mathbf{r}$ being the normalized vector particle-observer and $\beta = \mathbf{v}/c$. R is the distance particle-observer. Integration is performed over x' at retarded time $t' = t - \eta R/c$. The dependence in the air density ρ_{air} appears implicitely through the charge density ρ. The air refractive index drives the amplitude and arrival time of the electric field (it appears in the denominators of Eq. 1) i.e. the pulse shape, in particular close to the Cherenkov angle. It is therefore of prime importance to provide a realistic atmospheric model, which is not possible using the commonly-used US Standard description [8]. The details of the method are in [9].

2. Atmospheric model

As we experience daily, the atmosphere is a quickly varying medium with day/night effects and seasonal variations (winter/summer). The weather conditions also depend on the considered location on Earth. It is natural to use an atmospheric model that follows these variations.

2.1. The US Standard atmospheric model

It has been proposed in 1976 and it is an idealized modelisation of the atmosphere from an altitude of 0 up to 1000 km. The atmosphere characteristics are obtained from yearly averages assuming a hydrostatic equilibrium of the fluid. In this model, air is considered as a homogeneous mixture of various gases. The full height of the atmosphere is divided in 5 layers with some continuity conditions. Air density $\rho_{\mathrm{air}}(z)$ is a static average, valid for all locations on Earth, at all times (no day/night nor winter/summer influence). This very rough description of the atmosphere can lead to large deviations compared to actual weather conditions; and we can also expect some deviations in the resulting electric field from air showers. The code SELFAS used this parameterization until December 2016; then we switched to a more refined model, using the GDAS data.

2.2. The GDAS atmospheric model

GDAS [10] is the Global Data Assimilation System. It is the system used by "the Global Forecast System (GFS) model to place observations into a gridded model space for the purpose of starting, or initializing, weather forecasts with observed data." They produce a 3D model space that is based on ground observations, balloon measurements, satellite data, aircraft reports etc. Data are available from year 2001 on grids of various sizes ($1^\circ \times 1^\circ$, $0.5^\circ \times 0.5^\circ$ up to $0.25^\circ \times 0.25^\circ$) in longitude and latitude. The data is updated every 3 hours between the sea level up to an altitude of $z_{\mathrm{max}}^{\mathrm{GDAS}} = 26$ km. Many physico-chemical data are available but we need a small fraction of them to compute the air density and air refractive index above the observation site. These mandatory data are: the relative humidity R_h, the temperature T and the pressure P. As an illustration of the dynamics of the atmospheric conditions, we show in Fig. 1 the variation in relative humidity with time during a single day (March 18, 2014). We see very large variations that will affect in particular the air refractive index value: the pulse shape must be estimated using the air refractive index computed from the actual relative humidity and not an average value.

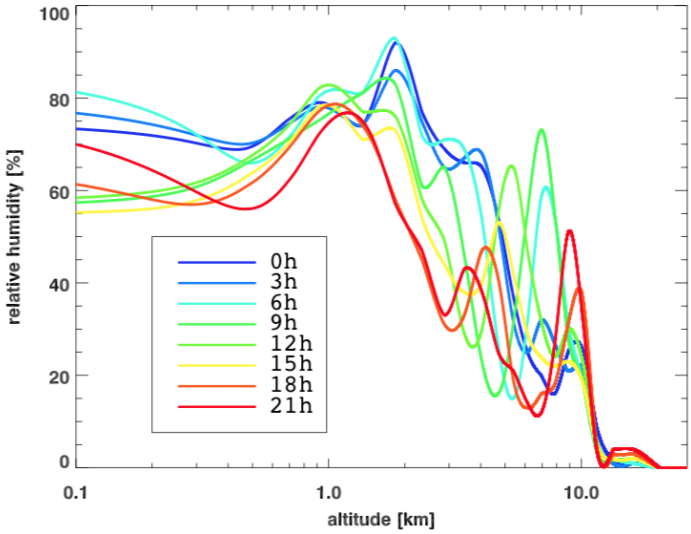


Figure 1. Relative humidity as a function of altitude above Nançay on March 18, 2014, for different time in the day.

2.3. Air density computation

The air density can be estimated using the ideal gas law:

$$\rho_{\text{air}}(z) = \frac{p_d(z(Z_g,\phi))M_d + p_v(z(Z_g,\phi))M_v}{RT(z(Z_g,\phi))},$$

where $z(Z_g,\phi)$ is the altitude above sea level, depending on the geopotential height Z_g at a latitude ϕ; p_d and p_v are the partial pressures of dry air and water vapor respectively; M_d and M_v are associated the molar masses. GDAS data are given as a function of Z_g that we can convert in altitude above sea level using:

$$z(Z_g,\phi) = \frac{g_0}{C}\left(\Lambda(\phi) - \sqrt{\Lambda^2(\phi) - \frac{2C\,Z_g}{g_0}}\right)$$

with:

$$\Lambda(\phi) = 1 + A\sin^2(\phi) - B\sin^2(2\phi)$$
$$\text{where } A = 0.0053024,\ B = 5.8\times10^{-6},\ C = 3.086\times10^{-6}\ \text{s}^{-2}.$$

We compute the water vapor partial pressure from $p_v = R_h\,p_{\text{sat}}$ where p_{sat} is given by (see [11, 12]):

$$p_{\text{sat}} = 6.1121\exp\left[\left(18.678 - \frac{T}{234.5}\right)\left(\frac{T}{257.14+T}\right)\right] \quad (T \text{ in } ^\circ\text{C}).$$

The dry air partial pressure is $p_d = P - p_v$. We can use these results in the range $[-80;+50]^\circ$C, which is precisely our range of interest.

At this stage, we know the air density ρ_{air} between sea level and $z_{\text{max}}^{\text{GDAS}} = 26$ km. Since we deal with air showers that can start to develop at much higher altitude, we need to extend the

$\rho_{\rm air}$ estimation up to the atmosphere limit of ~ 110 km. For altitude above $z_{\rm max}^{\rm GDAS}$, we use the US Standard model with a scaling factor to ensure continuity with our GDAS estimation of $\rho_{\rm air}$. This is possible as the atmosphere, above 26 km of altitude, is much more stable than at lower altitudes and the US Standard model is relevant. So in the end, we have the value of air density for all altitudes between sea level up to 110 km which can be seen as the limit of the atmosphere (i.e. where no shower can develop yet). Note that the relative difference $(\rho_{\rm air}^{\rm GDAS} - \rho_{\rm air}^{\rm US})/\rho_{\rm air}^{\rm US}$ when comparing the air density obtained the GDAS data or only the US Standard model can reach some tens of %. For instance, for the sample day of March 18, 2014, the maximum difference is of 15% for an altitude around 15 km. We can estimate the influence of such a difference on the electric field at ground level. For this, we simulate with SELFAS3 a shower with zenith angle $\theta = 30°$ and azimuth $\phi = 90°$ (i.e. coming from the North, azimuth are counted anti clockwise). The primary particle is a proton of 10^{18} eV (1 EeV) and the first interaction occurs at an atmospheric depth of $X_1 = 100$ g/cm^2. We ran the code with the very same shower once with the US Standard model, and another time with the actual atmospheric conditions of March 18, 2014 using the GDAS data. The difference in the total electric field amplitude is shown in FIG. 2. It is the amplitude in the horizontal direction $\mathbf{v} \times \mathbf{B}$ projected onto the ground frame, $\mathbf{v}$ being the shower axis direction and $\mathbf{B}$ the geomagnetic field at the observation site. In this

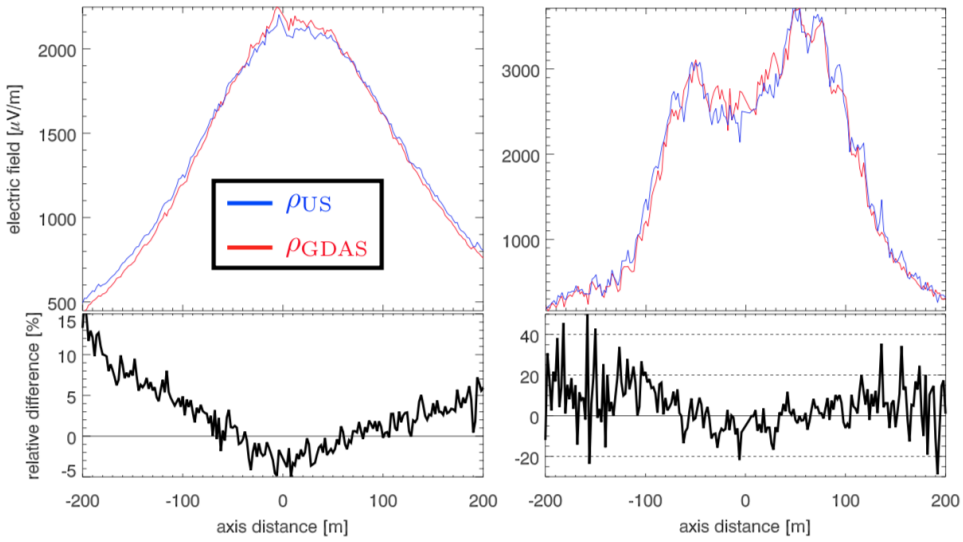


Figure 2. Electric field amplitude as a function of shower axis distance, in [20; 80] MHz (left) and [120; 250] MHz (right). The blue curve corresponds to the US Standard model ($\rho_{\rm air}^{\rm US}$) and the red curve to the refined model based on the GDAS data on March 18, 2014 at noon ($\rho_{\rm air}^{\rm GDAS}$). We show the relative difference between both models.

example, we see that the electric field profile is wider when using the US Standard model that will lead to a larger estimation of the shower $X_{\rm max}$. Using the US Standard model is a source of systematic uncertainties.

2.4. Air refractive index computation

The simulation codes usually take the Gladstone and Dale law to compute the air refractive index:

$$\eta(z(l)) = 1 + \kappa\, \rho_{\rm air}(z(\ell)) \text{ with } \kappa = 0.226 \text{ cm}^3/\text{g}.$$

We need to know the air refractive index value at the emission point. We also need its average value along the line of sight between the observer position and the emission point:

$$< \eta(z(\ell)) >= 1 + \frac{\kappa}{\ell} \int_0^\ell \rho_{\rm air}(z(\ell'))\, \mathrm{d}\ell'$$

We see that the air density also appears in this computation. The problem with the Gladstone and Dale law is that it is valid for optical wavelengths [13] and is not valid for our much larger wavelengths ($\lambda = 7.5$ m at 40 MHz). We use instead the relation proposed in [14], valid at high frequency (HF):

$$\eta = 1 + 10^{-6} N \quad \text{with} \quad N_{\rm HF} = \frac{77.6}{T}\left(P + 4810\,\frac{p_v}{T}\right) \qquad T \text{ in K},$$

where N is the refractivity. The relative humidity is taken into account through p_v so that we can estimate the refractivity $N_{\rm HF}^{\rm GDAS}$. At higher altitude, the relative humidity can be considered as null, as no clouds are usually observed above 12 km and the refractivity reduces to:

$$N_{\rm HF}^{\rm GDAS} = 77.6\,\frac{R\,\rho_{\rm air}}{M_d}$$

where $\rho_{\rm air}$ is the air density above $z_{\rm max}^{\rm GDAS}$ i.e. is given by $\rho_{\rm air}^{\rm US}$ with the scaling factor. The refractivity can be compared with different combinations: $N_{\rm GD}^{\rm GDAS}$ based on $\rho_{\rm air}^{\rm GDAS}$ and the Gladstone-Dale law, $N_{\rm GD}^{\rm US}$ based on $\rho_{\rm air}^{\rm GDAS}$ and the Gladstone-Dale law and $N_{\rm HF}^{\rm GDAS}$ based on $\rho_{\rm air}^{\rm GDAS}$ and the HF law. Tab. 1 presents the relative differences between all estimations. The

altitude (km)	$(N_{\rm GD}^{\rm GDAS} - N_{\rm GD}^{\rm US})/N_{\rm GD}^{\rm US}$	$(N_{\rm HF}^{\rm GDAS} - N_{\rm GD}^{\rm US})/N_{\rm GD}^{\rm US}$	$(N_{\rm HF}^{\rm GDAS} - N_{\rm GD}^{\rm GDAS})/N_{\rm GD}^{\rm GDAS}$	$(\eta_{\rm HF}^{\rm GDAS} - \eta_{\rm GD}^{\rm US})/\eta_{\rm GD}^{\rm US}$
0	$(1.3 \pm 4.35)\%$	$(18.1 \pm 24.0)\%$	$(16.5 \pm 5.0)\%$	$(5.0 \pm 6.6) \times 10^{-5}$
2.5	$(-0.1 \pm 1.6)\%$	$(6.5 \pm 11.0)\%$	$(6.6 \pm 4.3)\%$	$(1.4 \pm 2.4) \times 10^{-5}$
5	$(-0.4 \pm 1.0)\%$	$(1.4 \pm 3.5)\%$	$(1.76 \pm 2.2)\%$	$(2.3 \pm 5.8) \times 10^{-6}$
7.5	$(0.3 \pm 1.4)\%$	$(0.2 \pm 1.3)\%$	$(-0.17 \pm 1.2)\%$	$(1.2 \pm 16.7) \times 10^{-7}$
10	$(0.3 \pm 3.2)\%$	$(-0.8 \pm 2.2)\%$	$(-1.1 \pm 3.0)\%$	$(-7.2 \pm 20.3) \times 10^{-7}$
12.5	$(0.6 \pm 6.1)\%$	$(-0.8 \pm 4.7)\%$	$(1.35 \pm 5.6)\%$	$(-6.0 \pm 29.8) \times 10^{-7}$
15	$(0.6 \pm 5.3)\%$	$(-0.8 \pm 3.9)\%$	$(-1.4 \pm 4.8)\%$	$(-3.6 \pm 16.7) \times 10^{-7}$
17.5	$(0.6 \pm 4.8)\%$	$(-0.8 \pm 3.3)\%$	$(-1.4 \pm 4.2)\%$	$(-2.4 \pm 9.5) \times 10^{-7}$
20	$(0.6 \pm 4.0)\%$	$(-0.8 \pm 2.5)\%$	$(-1.4 \pm 3.4)\%$	$(-2.4 \pm 4.8) \times 10^{-7}$

Table 1. Relative differences of the refractivity (N) and the refractive index (η) between several GDAS-based and US Standard-based models for several altitudes of interest for air showers physics. For GDAS-based models all the data of the year 2014 at Nançay were used to compute the mean differences along the year. The errors show the standard deviation at each altitude.

relative difference with the canonical estimation $N_{\rm GD}^{\rm US}$ (i.e. used in most simulation codes) can reach some tens of %. For the day of March 18, 2014, the relative difference reaches 35% at sea level and 15% at altitudes of interest for shower development, around 20 km. The relative difference on the air refractive index is smaller because of the 10^{-6} factor and the effect on the electric field is of the order of some % in the amplitude in 20-80 MHz and can reach 40% in 120-250 MHz. In conclusion, one should be cautious with the model for the refractive index when considering frequencies above ~ 100 MHz.

3. $X_{\rm max}$ reconstruction

We can study the influence of the models chosen for both air density $\rho_{\rm air}$ and refractivity N on simulated showers. We ran simulations to test 6 differents configurations of $(\rho_{\rm air}, N)$. For

data set	air density	air refractive index	ΔX_{30° [g/cm^2]
#1	US Std.	US Std. + GD	34.1 ± 8.9
#2	GDAS	US Std. + GD	5.7 ± 5.4
#3	GDAS	GDAS + GD	4.6 ± 3.6
#4	GDAS	GDAS + HF	0.1± 2.4
#5	GDAS	GDAS + HF (N+10%)	2.9 ± 4.8
#6	GDAS	GDAS + HF (N+20%)	9.3 ± 16.4

Table 2. Quality of the $X_{\max}$ reconstruction for 6 different configurations of air density and air refractive index. The ΔX column presents the mean difference with the true value and the 1σ deviation. GD stands for Gladstone-Dale.

each of these configurations, we used 10 iron showers and 40 proton showers with random $X_{\max}$ coming from $\theta = 30^\circ$, $\phi = 90^\circ$. In Tab. 2, we show the result of the comparison. The reference configuration is #4: $\rho_{\text{air}}^{\text{GDAS}}$ and $N_{\text{HF}}^{\text{GDAS}}$, which uses the most refined information to compute these quantities. We consider the electric field computed by each of the simulated showers of #4. Using this electric field pattern at ground level, we apply to procedure of [15] to reconstruct the $X_{\max}$, from the 50 showers simulated using the air density and refractivity model of the other configurations #1, #2, #3, #5, #6 and the 49 remaining independent showers of #4. We then get the average and standard deviation of the obtained $X_{\max}$ values and this is shown in the last column of Tab. 2.

This shows that using the most refined model gives an error on $X_{\max}$ compatible with zero ($0.1\pm$ 2.4 g/cm^2). We conclude by saying that the choice of the atmospherical model for ρ_{air} is critical for the $X_{\max}$ estimation. The choice of the refractivity model has a smaller impact on $X_{\max}$.

4. Conclusion

The source of ultra-high energy cosmic rays is still unknown. We hope that a much more precise measurement of the composition will help into understanding this old problem in astrophysics. Both the Pierre Auger Observatory and the Telescope Array will proceed to a significant upgrade of their instruments in this direction. The radio signal will also play a key role in the determination of the nature of the cosmic rays, since it can provide the shower $X_{\max}$ with competitive uncertainties, of the same order of what a fluorescence telescope can do ($X_{\max}$ resolution of ~ 19 g/cm^2 at 1 EeV, with systematic uncertainties of $+8/-13$ g/cm^2, see [16]) but with a $\sim 100\%$ duty cycle. To reach its best performances, the simulation codes that compute the expected electric field emitted by air showers should use a precise atmospheric model for both the air density and air refractive index. This can be achieved using the GDAS data and using a refractive index valid at the frequencies of interest (i.e. some tens of MHz). With these detailed models, the shower $X_{\max}$ can be retrieved with no systematic bias, as it is the case when using basic models. The code SELFAS3 uses the GDAS data and the correct law for the refractive index.

Acknowledgments

We thank the Région Pays de la Loire for its financial support of the Astroparticle group of Subatech and in particular for its contribution to the EXTASIS experiment.

References

[1] B. Revenu for the CODALEMA/EXTASIS collaboration. Current status of the CODALEMA/EXTASIS experiments. In *Proceedings of the 26th E+CRS/35th RCRC*, number 268, July 2018.

[2] E. Holt for the for the Pierre Auger Collaboration. Recent Results of the Auger Engineering RadioArray (AERA). In *ICRC2017*, volume 301, 2017.
[3] F. G. Schröder for the Tunka-Rex collaboration. Overview on the Tunka-Rex antenna array forcosmic-ray air showers. *PoS*, ICRC2017:459, 2018.
[4] Vincent Marin and Benoît Revenu. Simulation of radio emission from cosmic ray air shower with SELFAS2. *Astropart.Phys.*, 35:733–741, 2012.
[5] J. Alvarez Muñiz, W. R. Carvalho Jr, and E. Zas. Monte carlo simulations of radio pulses in atmospheric showers using ZHAireS. *Astropart. Phys.*, 35:325–341, 2012.
[6] T. Huege and C. James. Full Monte Carlo simulations of radio emission from extensive air showers with CoREAS. In *proceedings of the 33rd ICRC, Rio de Janeiro, Brasil*, number id 548. arXiv:1307.7566, July 2013.
[7] Daniel García-Fernández, Benoît Revenu, Didier Charrier, Richard Dallier, Antony Escudie, and Lilian Martin. Calculations of low-frequency radio emission by cosmic ray-induced particle showers. *Phys. Rev.*, D97(10):103010, 2018.
[8] NASA NOAA. https://ntrs.nasa.gov/archive/nasa/casi.ntrs.nasa.gov/19770009539.pdf. Technical report, 1976.
[9] F. Gaté, B. Revenu, D. García-Fernández, V. Marin, R. Dallier, A. Escudié, and L. Martin. Computing the electric field from extensive air showers using a realistic description of the atmosphere. *Astroparticle Physics*, 98:38 – 51, 2018.
[10] GDAS Archive Information, http://ready.arl.noaa.gov/gdas1.php. Technical report, NOAA.
[11] A. L. Buck. New equations for computing vapor pressure and enhancement factor. *J. Appl. Meteorol.*, (20):1527:1532, 1981.
[12] A. L. Buck. Buck research cr-1a user's manual. Technical report, 1996.
[13] W. Merzkirch. *Flow Visualization (Second Edition)*. Number ISBN: 978-0-12-491351-6. Elsevier, 1987.
[14] R. L. Freeman. *Radio System Design for Telecommunications, Third Edition*. 2006.
[15] Lilian Martin, Richard Dallier, Antony Escudie, Daniel García-Fernández, Florian Gaté, Alain Lecacheux, and Benoît Revenu. Main features of cosmic ray induced air showers measured by the CODALEMA experiment. *PoS*, ICRC2017:414, 2018.
[16] Pierre Auger Collaboration and Alessio Porcelli. Measurements of xmax above 1017 ev with the fluorescence detector of the pierre auger observatory. In *34th International Cosmic Ray Conference, ICRC 2015, The Hague, NL, July 30 - August 6, 2015*, Proceedings of Science, page Art.Nr.: 420. SISSA (International School for Advanced Studies), Triest, 2016. 51.03.03; LK 01.